Soft Matter

Mechanical properties of bulk graphene oxide / poly(acrylic acid) / poly(ethylenimine) ternary polyelectrolyte complex

Journal:	*Soft Matter*
Manuscript ID	SM-ART-01-2018-000176.R2
Article Type:	Paper
Date Submitted by the Author:	03-May-2018
Complete List of Authors:	Duan, Yipin; University of Akron, Polymer Engineering Wang, Chao; University of Akron, Polymer Engineering Zhao, Mengmeng; University of Akron, Polymer Engineering Vogt, Bryan; University of Akron, Polymer Engineering Zacharia, Nicole; University of Akron, Polymer Engineering; Texas A&M, Mechanical Engineering

Soft Matter

ARTICLE

Mechanical properties of bulk graphene oxide / poly(acrylic acid) / poly(ethylenimine) ternary polyelectrolyte complex

Received 00th January 20xx,
Accepted 00th January 20xx

DOI: 10.1039/x0xx00000x

www.rsc.org/

Yipin Duan, Chao Wang, Mengmeng Zhao, Bryan D. Vogt,* and Nicole S. Zacharia*

Ternary complexes formed in a single pot process through the mixing of cationic (branched polyethylenimine, BPEI) and anionic (graphene oxide, GO, and poly(acrylic acid), PAA) aqueous solutions exhibit superior mechanical performance in comparison to their binary analogs. The composition of the ternary complex can be simply tuned through the composition of the anionic solution, which influences the water content and mechanical properties of the complex. Increasing the PAA content in the complex decreases the overall water content due to improved charge compensation with the BPEI, but this change also significantly improves the toughness of the complex. Ternary complexes containing ≤ 32 wt % PAA were too brittle to generate samples for tensile measurements, while extension in excess of 250 % could be reached with 57 wt % PAA. From this work, the influence of GO and PAA on the mechanical properties of GO/PAA/BPEI complexes were elucidated with GO sheets acting to restrain the viscous flow and improve the mechanical strength at low loading (<12.6 wt%) and PAA more efficiently complexes with BPEI than GO to generate a less swollen and stronger network. This combination overcomes the brittle nature of GO-BPEI complexes and viscous creep of PAA-BPEI complexes. Ternary nanocomposite complexes appear to provide an effective route to toughen and strengthen bulk polyelectrolyte complexes.

1.Introduction

Oppositely charged ion-bearing polymers are thermodynamically driven to strongly associate with one another to form polyelectrolyte complexes (PECs) when mixed in solution.[1, 2] Complexation is generally considered favourable because the association of oppositely charged macromolecules releases small counterions into solution, increasing the entropy of the system.[3] At charge ratios generally approaching the stoichiometric match of the polyanion and polycation, complexation results in a solid precipitate.[4] This type of precipitate is the subject of investigation in this work, rather than soluble complexes created by highly non-stoichiometric ratios of oppositely charged macromolecules. This resultant solid material is an ionically crosslinked network, generally swollen with water, but to a lesser extent than hydrogels. In addition to precipitate, complexation can also result in soluble materials or a liquid-liquid phase separation known as coacervation. Complexation can also occur between polyelectrolytes and other polyvalent objects, such as colloidal particles or nanomaterials, with slightly different results.[5-7] For example, our group has reported mechanically adaptive materials based on solution assembly of graphene oxide (GO) and branched polyethylene imine (BPEI).[7] This material formed by complexation in aqueous solution is akin to a hydrogel, with 95% or greater water content. Alternatively, this complexation process can be driven to a surface to form films or coatings, a process of sequential exposure of the surface to oppositely charged solutions known as the layer-by-layer (LbL) method.[8] Nanomaterial-containing PECs and LbL films have gained a considerable interest in a number of potential applications such as drug delivery,[4,9, 10] energy storage,[11, 12] or gas barrier,[13] due to their excellent properties.[14, 15] Although LbL is a good technique for creating thin films and surfaces, it has some disadvantages, including that it is time consuming and potentially difficult to scale up.[16] On the other hand, formation of bulk PEC by simply mixing solutions can be a simple and efficient route to large quantities of materials, sometimes with different properties compared to the thin films and surfaces formed by LbL.[8, 17] This solution mixing has been shown to be an efficient route to bulk polyelectrolyte complex based materials that can be processed using traditional methods such as extrusion, when plasticized with water or salt.[18]

Other studies reporting bulk PEC nanocomposites created from solution assembly largely focus on binary systems of polyelectrolyte and nanomaterial, with applications such as dye absorbence,[19, 20] gene delivery carrier,[21] and electrode materials.[22] In some cases, the hydrogel like material formed between polyelectrolyte and nanomaterial is dried to create a porous material.[13] The charge-charge interactions between the polyelectrolyte and the nanomaterial helps to disperse the nanomaterial. The mechanical and tensile properties of these binary complexes are less well reported, probably due to the fact that these materials tend to be brittle.[23, 24] In one exception, Fu, et al. have reported a polyelectrolyte nanocomposite complex material made from a ternary mixture of Fe_3O_4, polydimethyldiallylammonium chloride, and sulfonated polystyrene.[24] This material has an ultimate strength up to 15 MPa, which is superior compared to other PEC materials[25, 26] that generally have ultimate strengths lower than 5 MPa. The ternary mixture has some degree of stretchability as well.[24] This

Department of Polymer Engineering, University of Akron, 250 S. Forge St, Akron OH 44325

Electronic Supplementary Information (ESI) available. See DOI: 10.1039/x0xx00000x

study demonstrates the possibility of incorporating nanomaterials with two oppositely charged polyelectrolytes in order to form a PEC material with a wider range of mechanical properties.

Previous studies on the binary complex of GO and BPEI show that the material has high mechanical strength (~3.62 MPa plateau modulus) and also exhibits mechanically adaptive behavior upon compression.[7] These properties make possible potential applications for the GO/BPEI complex in energy dissipation and sensing. However, the limited extensibility narrows these applications. In the present work, bulk GO/poly (acrylic acid) (PAA)/BPEI ternary PEC nanocomposites were produced from solution assembly. The influence of the ratio of the two negatively charged components, PAA and GO, on the mechanical properties was investigated. The ternary PEC materials exhibited better tensile properties and processability when compared to the GO/BPEI binary complex materials, had a better resistance to viscous flow than PAA/BPEI complexes under only the influence of its own weight and gravity, and are more resilient against creep under a tensile load. These ternary materials have better have better processability compared to the binary GO containing system previously studied. A change from gel to near critical-gel behavior was also observed as the PAA content was increased and exceeded GO content in the complex. Understanding of the role of PAA chains and GO sheets in toughening of the GO/polyelectrolyte complex hydrogels will be helpful for designing functional PECs by incorporating 2D nanomaterials.

2.Experimental Methods

2.1 Materials

Branched poly(ethylenimine) (BPEI, average M_w = 25 000 g/mol, PDI = 3.09), graphite (powder, < 45 μm, ⩾ 99.99%), potassium permanganate ($KMnO_4$, ⩾ 99.0%), hydrochloric acid (HCl, 37% aq.), phosphoric acid (H_3PO_4, ⩾ 85 wt% aq.), deuterium oxide (D_2O, 99.9 atom % D), deuterium chloride (DCl, 35 wt% in D_2O, 99 atom % D), sodium hydroxide (NaOH, ⩾ 98%) and potassium bromide (KBr, ⩾ 99%) were purchased from Sigma-Aldrich Chemical Co. Sulfuric acid (H_2SO_4, 95-98%) and hydrogen peroxide (H_2O_2, 30% solution) were purchased from VWR. Poly(acrylic acid) (PAA, M_w = 50 000 g/mol, PDI = 5.42, 25 wt% aq.) was purchased from Polysciences, Inc. Deionized (DI) water with resistivity of 18.2 MΩ used in the experiments was purified by a Milli-Q DQ-3 system (Millipore, Bedford, MA, U.S.A.). All chemicals were used as received.

2.2 Synthesis and characterization of graphene oxide (GO)

The GO was synthesized using the modified Hummer's method.[27] To be brief, a mixture of concentrated H_3PO_4 (⩾ 85 wt% aq.) / H_2SO_4 (95-98%) (20 ml：180 ml) was gently added to $KMnO_4$ (9 g) and graphite flakes (1.5 g) under stirring. The reaction proceeded under mechanical stirring at 50 °C for 12 h. The mixture was then poured onto ice (~200 mL) made from DI water. H_2O_2 (30% solution) was added under stirring to remove the excess $KMnO_4$. The resulting mixture was repeatedly washed with DI water and then solid was separated by centrifugation, until the pH of supernatant reached 6.0-7.0. Finally, the product was redispersed in DI water by sonication for 30 min to obtain stable GO suspension with known concentration.

The synthesized GO was analyzed by Raman spectroscopy on a Horiba LabRam HR Micro Raman Spectrometer. Both the in-phase vibration[28] of the graphene lattice (G band) at 1575 cm^{-1} and the disorder band[28] which are a sign of the graphene edges at 1355 cm^{-1} can be observed, Fig S1(a). Fourier transform infrared spectroscopy was performed using a Thermo Scientific iS50 FT-IR to provide information about the chemical bonds of the graphene oxide samples. The specimen was loaded onto the sample stage (Praying Mantis Sampling Kit, DRP-SAP, Harrick Scientific Products, Inc.) in a reaction chamber (DRK-3-NI8, Harrick Scientific Products, Inc.) for the FTIR analysis. The measurement was performed in reflection mode, with a resolution of 4 cm^{-1} and 256 scans for the sample. The broad peak from ~2492 cm^{-1} to ~3715 cm^{-1}, Fig S1(b), is attributed to the O-H stretch from water or the carboxyl and hydroxyl groups on GO.[29] The peak at ~1755 cm^{-1} is attributed to the C=O stretch of the carboxylic group on GO.[29]

The size of the synthesized GO was characterized by dynamic light-scattering (DLS) measurements using a Zeta PALS instrument. The measurement temperature was 25 °C. All analyses were performed with the instrument software. The hydrodynamic diameter of the synthesized GO is 1820 ± 167 nm.

2.3 Complexation of GO/PAA/BPEI

The nomenclature for the concentrations of the solutions is $[component]_{sol}$ to differentiate from the concentrations in the complex. To prepare the polyanion solution, the desired amount of PAA was first added into GO suspension (2 mg / ml). The mixture was then stirred overnight and sonicated for 15 min before being diluted by DI water in a volumetric flask. The diluted mixture was again stirred overnight to obtain a homogeneous mixture of GO/PAA ($[GO]_{sol}$ = 1 mg / ml, $[PAA]_{sol}$ = 0-280 mM with respect to carboxyl group of PAA). For the polycation solution, $[BPEI]_{sol}$ = 200 mM with respect to amine group of BPEI was prepared in DI water. The pH of GO / PAA mixture and BPEI solution were adjusted to 2.5 and 11.0, respectively, using dilute NaOH and HCl. The selected pH values are close to the pH of the solutions as the materials are dissolved/suspended in DI water to minimize the effect of added salt formed by adjusting pH with acid or base solutions.[25, 30] At these values, PAA is nearly completely protonated and BPEI nearly completed deprotonated, however weak polyelectrolytes are known to change their degree of protonation when they come in close proximity with opposite charges. The GO/PAA/BPEI complex was obtained by simultaneously mixing polyanion solution with polycation solution (100 ml / 100 ml) under stirring. The mixture was stirred for 15 min and then allowed to rest for 1 h to allow the precipitate or complex to settle, followed by DI water wash to remove the soluble complex. The resultant materials after

washing are solid complexes instead of coacervates (liquid-liquid separation). Native complexes were compression molded into 1.25 mm-thick flat sheets and then swollen in DI water at room temperature for at least 48 h before characterization to ensure that equilibrium was obtained. A schematic of the protocol to fabricate GO/PAA/BPEI complex is shown in Fig 1. A PAA/BPEI complex was also prepared for comparison. The fabrication protocol is same as GO/PAA/BPEI complex, except using PAA as the only component in polyanion solution ($[PAA]_{sol}$ = 200 mM). DI water was used to swell the GO/PAA/BPEI complex for 24 hours and also periods of three months were examined by UV-vis spectroscopy using an Agilent 8453 UV–vis Spectrophotometer. No significant loss of material was observed during swelling, Fig S2.

2.4 Physical characterization

The equilibrium mass swelling ratio (q) of the GO / PAA / BPEI complex was defined as (mass of fully swollen complex)/(mass of dried complex). The swollen complex was determined to be in equilibrium when the change in mass over 24 h while soaking in DI water was less than 5%. Similarly, the complex was dried in a vacuum oven at 30 °C for at least 72 h and determined to be fully dry when there was less than 5% change in mass after further drying at same condition. Solution state ^{1}H NMR spectroscopy (Varian MERCURY 300 MHz spectrometer) was used to determine the ratio of BPEI : PAA in the complex. For NMR, small pieces of the dried complex (15-25 mg) were dissolved in 0.5 mL D_2O solution containing 2.5 M KBr and 3.5 wt% DCl. The individual GO, PAA and BPEI were prepared using the same method for controls. As shown in Fig S3., the spectrum of the dissolved complex is the combination of individual BPEI and PAA, while GO has no contribution to the signal from 0.5 to 4.5 ppm. We attributed the signal from 3.0 to 4.0 ppm to the protons on -CH_2- groups on BPEI and signal from 1.25 to 2.5 ppm to the protons on the backbones of PAA. The mass ratio (m : m) of BPEI : PAA (R) is calculated by the equation (1).

$$\boldsymbol{R} = \frac{\boldsymbol{m(BPEI)}}{\boldsymbol{m(PAA)}} = \frac{\boldsymbol{A_{(3.0-4.0\,ppm)} \div 4 \times M_{(BPEI)}}}{\boldsymbol{A_{(1.25-2.5\,ppm)} \div 3 \times M_{(PAA)}}} \quad (1)$$

where $\boldsymbol{A_{(3.0-4.0\,ppm)}}$ and $\boldsymbol{A_{(1.25-2.5\,ppm)}}$ refer to integral area calculated from 3.0 to 4.0 ppm and from 1.25 to 2.5 ppm; $\boldsymbol{M(BPEI)}$ and $\boldsymbol{M(PAA)}$ refer to the mole mass of repeat unit of BPEI and PAA. Thermal gravimetric analysis (TGA, TA instruments Q50 Thermogravimetric Analyzer) was performed on the dried complex on heating from 30 °C to 800 °C at 10 °C/min under N_2 purge. TGA data for individual components of GO, PAA and BPEI were collected under same condition. As shown in Fig S4a., BPEI is completely removed from the complex at 600 °C. Based on the TGA curves of dried complexes (Fig S4b), considering the amount of water can be neglected, when PAA wt% = x, BPEI wt% = Rx, GO wt% = (100% - x – Rx), the composition of the complexes should satisfy equation (2).

$$\mathrm{W}_C(T) = \mathrm{W}_P(T) \cdot x + \mathrm{W}_G(T) \cdot (100\% - x - Rx) \quad (2)$$

where $\boldsymbol{W_C(T)}$, $\boldsymbol{W_P(T)}$ and $\boldsymbol{W_G(T)}$ are the mass remaining of dried complex, individual PAA and individual GO at T °C (T = 600-800), respectively. The average value of composition and its standard deviation are calculated from the composition data obtain at 600-800 °C. The weight percent of PAA, GO and BPEI in the dried complex is referred as [PAA], [GO] and [BPEI], respectively, henceforth.

2.5 Mechanical tests

To perform tensile tests, dumbbell-shaped tensile bars were cut from the fully swollen flat sheets of the complexes using a ASTM D-638 Type V die. The samples were stretched by a texture analyzer (TA-TX plus) with an extension rate of 10 mm / min (strain rate of 1.3%/sec). For each composition of the complexes, three specimens were tested for reproducibility. All measurements were performed at 25 °C and ~50% relative humidity. The elastic modulus (E) was calculated as the slope of the initial linear region in the stress-strain curve. The toughness (U_T) was calculated by integrating the area under the stress–strain curve.

The rheology of 8 mm diameter disk-shaped samples cut from the fully swollen flat sheet was elucidated using a TA instrument ARES-G2 rheometer, with an 8 mm upper plate and a 43.9 mm lower plate equipped with a water trap. All of the rheological measurements were performed with 10 ml of DI water in the water trap to prevent the dehydration of the complex. To determine the linear viscoelastic (LVE) response region, a strain sweep from 0.1% to 100% at 1.0 rad/s was performed. Angular frequency sweeps data from 0.1 to 100.0 rad/s were obtained at a constant strain amplitude of 0.50%, which was within the region for LVE response for all complexes examined.

2.6 Contact angle measurement

All contact angle measurements were taken on a VCA-optima contact angle goniometer (AST products) equipped with a tilting stage at ambient condition. Static contact angle measurements were performed by slowly placing 2 μl Type 1 ultrapure water (Milli-Q, Millipore Corp.) droplet onto the flat sheets of complexes sample. The contact angle was then measured by fitting the outline of the droplet using the VCA software. All measurements were repeated at three different spots on the substrate and averaged.

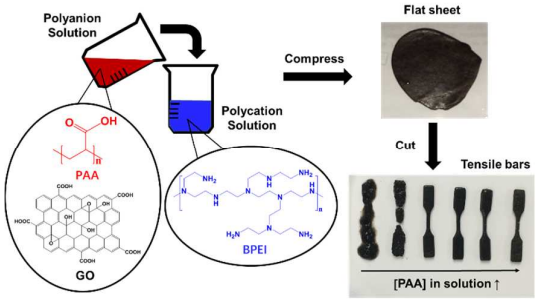

Fig 1. Schematic illustrating the protocol to fabricate the GO/PAA/BPEI complex and to prepare the samples for tensile tests.

3. Result and discussion

3.1 Influence of mixing condition on composition and processability of GO/PAA/BPEI complexes

Within the PECs, polymer chain mobility is much more constrained than in solution, making it difficult to achieve a one to one matching of the opposite charge groups.[31] For this reason, polyelectrolyte based materials, such as polyelectrolyte multilayers, often exist in a kinetically trapped state. Since the stoichiometry of the resultant material is influenced by factors such as the initial mixing or feed ratio, mixing speed, as well as the nature of the components and their interactions, it remains difficult to predict the composition of the precipitate from the feeding condition alone.[31, 32] For GO/PAA/BPEI complexes, some thermodynamic insights may be provided from the examination of the three binary aqueous systems. At 1 mg/mL of GO, a single-phase system was observed when mixed with PAA at all concentrations examined. This is expected as the PAA and GO are both negatively charged. At the same concentration of GO, Duan *et al*. have previously reported that the binary system of GO and BPEI tend to phase separate even when the BPEI concentration is quite small (0.010 wt%).[7] The mixture of PAA and BPEI in water solution only leads to either the formation of soluble complexes or complex coacervation coacervation (liquid-liquid phase separation) at off stoichiometric ratios, while solid complexes or precipitates are formed with near stoichiometric ratios.

TGA and NMR were used to further estimate the composition of the precipitated materials. Fig S5 and Table 1 summarize the composition of the complexes. As shown in Fig S5, with $[PAA]_{sol}$ increasing from 40 to 280 mM, the [PAA] in the precipitate increases. As both PAA and GO are negatively charged, GO sheets compete with PAA to interact with the positively charged BPEI. In studies mixing polyanions to form polyelectrolyte multilayers, it is seen that rather than a mixture of polyanions matching the solution composition, one polyanion will preferentially bind with the polycation.[33, 34] As the $[PAA]_{sol}$ becomes proportionately larger with $[GO]_{sol}$ constant (1 mg/mL) for all the samples, [GO] in the dried complex decreases. [GO] decreases sharply when $[PAA]_{sol}$ increases from 40 to 120 mM; then it shows a smaller decrease when $[PAA]_{sol}$ further increases to 200 mM; finally, when $[PAA]_{sol}$ increases from 200 mM to 280 mM, [GO] appears to slightly increase, as shown in Table 1. At high $[PAA]_{sol}$, PAA chains might interact with GO through hydrogen bonding[35] or physical entanglement, trapping GO sheets within the complex and resulting in the slight increase in [GO]. On the other hand, [BPEI] is almost independent to the feeding amount of PAA and fluctuates between 26 - 35 wt%.

Table 1. Compositions of dried GO/PAA/BPEI complex estimated from TGA and NMR

$[PAA]_{sol}$ (mM)	Dried complex composition (wt%)		
	BPEI	PAA	GO
40	30.5 ± 4.6	20.9 ± 3.2	48.6 ± 7.8
80	26.8 ± 3.0	32.5 ± 4.1	40.7 ± 7.1
120	35.7 ± 1.8	44.1 ± 2.2	20.1 ± 4.0
160	34.5 ± 0.9	47.9 ± 1.3	17.6 ± 2.2
180	32.7 ± 0.4	50.3 ± 0.6	17.0 ± 0.9
200	35.5 ± 0.2	52.9 ± 0.3	11.6 ± 0.4
220	32.2 ± 0.2	55.5 ± 0.3	12.3 ± 0.5
240	32.5 ± 0.6	55.1 ± 1.1	12.4 ± 1.7
280	29.5 ± 0.3	57.9 ± 0.5	12.5 ± 0.7

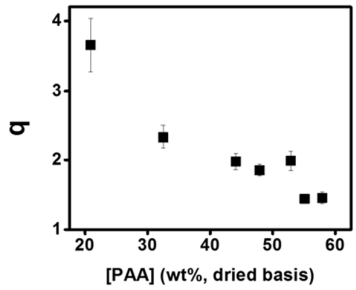

Fig 2. Equilibrium mass swelling ratio (q) of GO/PAA/BPEI complex as a function of the PAA concentration in the dried complex

The carboxyl group content on the GO sheets was 1.35 mmol/g from titration.[7] Compared to the functionality of PAA (13.89 mmol/g, calculated from its chemical structure), GO has a lower carboxyl group density. The amine group density on the BPEI is 23.26 mmol/g from stoichiometry, with on average 25% tertiary amines, 50% secondary amines, and 25% primary amines. Considering that the amount of positively charged BPEI in the complex remains approximately the same, the increasing [PAA] means that a higher fraction of the amine groups on BPEI are occupied by PAA. A higher ionic crosslink density created by more acid groups on the PAA binding with amine groups from BPEI leads to a less water swollen material, and decreased hydration of the complex.[36] As the density of charges along BPEI and PAA backbones are similar, the PAA can better compensate the charges on the BPEI chain as opposed to the GO where the charges are more distributed. This is consistent with the equilibrium mass swelling ratio (q)

(defined as the mass of swollen material divided by the mass of dried material and shown in Fig 2); as the [PAA] in the precipitate increases, *q* decreases. Fig 3 shows the static water contact angle on the surface of the fully hydrated complex precipitates that have been pressed flat to avoid artifacts from topography. In general, it can be seen that the inclusion of GO increases the contact angle of the material, indicating that the inclusion of these hydrophobic particles does change the material's surface properties. For a polyelectrolyte-only complex, the contact angle is just over 60°, but for the GO containing materials can be as high as 85°. Also, as overall water content (thus, *q*) is increased, the static water contact angle decreases, as one would expect, but the GO containing complex has a higher contact angle than the polyelectrolyte-only complex, even when the GO containing complex has much higher water content. This is attributed to the interplay between the intrinsic hydrophobicity of the graphene that comprises a majority of the GO and the swelling from uncompensated charges on the BPEI.

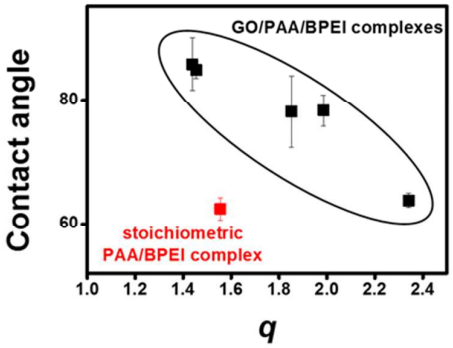

Fig 3. Contact angle of different GO containing materials.

The composition of the hydrated complex also has an influence on the physical properties and processablity of the materials. For the complexes with a [PAA] lower than 44 wt% ($[PAA]_{sol}$ < 120 mM), the resultant materials were so fragile and brittle that no matter how carefully handled, they would be broken when being cut into tensile bars or loaded onto the clamps of the testing instrument. This fragility prohibited the acquisition of tensile properties for these samples. However, increasing [PAA] can largely improve the processability of the complexes. As shown in Fig 1, samples with higher PAA content were less fragile and able to be molded into desired shape without breaking.

3.2 Rheological properties of GO/PAA/BPEI complexes

Variation in rheological behaviour of complexes can provide insight into the microstructure of the complex as a function of composition. Fig 4a shows how G' and G'' of the complexes at 1 rad/s are impacted by [PAA]. Both G' and G'' increase with increasing [PAA]. This can be interpreted as the effect of the change in both crosslink density and hydration extent. As discussed in last section, the equilibrium swelling ratio *q* is associated with the PAA content in the dried material. Due to both increased flexibility of PAA chains compared to rigid GO particles as well as increased density of negative charges along the PAA backbones compared that of GO particles, PAA can form a larger density of ion pairs with BPEI than the GO particles can. This results in a decrease in equilibrium mass swelling ratio and an increase in crosslink density simultaneously. The increased crosslink density leads to a mechanically stronger network structure. Additionally, since water acts as a plasticizer within PECs[37, 38] with the ability to weaken or dissolve the ionic bond pairs, meaning that a decrease in swelling ratio would also contribute to the increase of shear storage moduli.

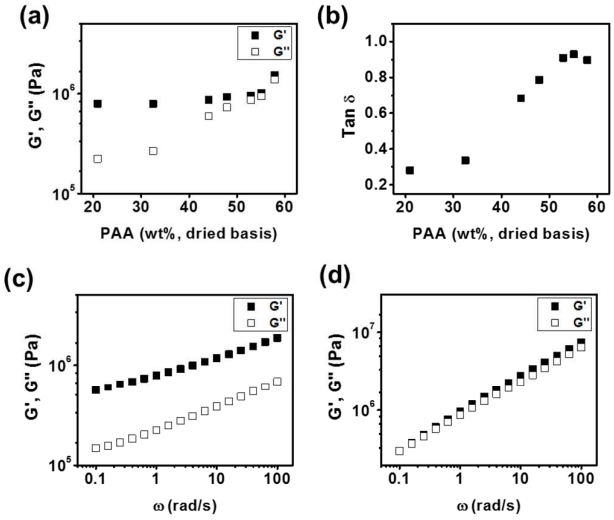

Fig 4. At ω = 1 rad/s, (a) storage modulus, G', (■) and loss modulus, G'', (□), (b) tan δ of GO/PAA/BPEI complexes with q = 1.45-3.66; G' (■) and G'' (□) of GO/PAA/BPEI complexes as a function of frequency when (c) $[PAA]_{sol}$ = 40 mM and (d) $[PAA]_{sol}$ = 200 mM

Based on the plasticization mechanism of water suggested by Hariri et al.,[38] the decrease in swelling ratio should occur concurrently with a decrease in chain mobility, making the material more solid-like. A higher crosslink density should also increase the elastic response of the materials. However, as shown in Fig 4a., the difference between G' and G'' decreases as [PAA] increases and the complex become less hydrated. The increase in G'' as [PAA] increases is associated with the ability of the complex to dissipate energy. The intrinsic rigidity of the GO appears to limit the viscous losses at 1 rad/s, while the pure BPEI/PAA complex when swollen with water is a viscoelastic liquid (G'' > G') at 1 rad/s so the addition of the PAA would be expected to increase the viscous losses.[25] This effect can also be seen from Fig 4b, which shows the loss factor (tan δ) of the complex as a function of [PAA]. The increase in [PAA] from 20.9 wt% to 57.9 wt% was accompanied with an increase in tan δ from 0.2 to 1.0, indicating the viscoelastic behaviour of the GO/PAA/BPEI was changing from solid-like towards liquid-like. Fig 4a and Fig 4b illustrate two

typical types of frequency (ω) dependent behaviour of the dynamic storage modulus (G') and loss modulus (G'') of GO/PAA/BPEI complex (frequency sweep plots of all the other samples are shown in Fig S6., ESI). At low [PAA], where GO is the dominant negatively charged molecule in the complex, as shown in Fig 4c, G' is greater than G'' at every frequency, indicating a solid-like behaviour of GO/PAA/BPEI complexes. While at high [PAA], G' is similar to G'' (Fig 4d). This rheological behaviour is similar to "critical gel" composition for gelating solutions, indicative of the sol-gel transistion.[39]

Subjected to oscillatory shear force, the ionically paired PAA-BPEI chains can dissipate energy from friction between chains and change of conformation, contributing to the viscous response; while limited by the platelet-like morphology of GO, the viscous response of ionic pair of GO-BPEI would be weaker. Thus, when [PAA] in the complex increases, more energy can be dissipated by the flexible and entangled polymer chains to make the complexes become more liquid-like, even though the water content (swelling ratio) is significantly reduced.

3.3 Tensile properties of GO/PAA/BPEI complexes

Uniaxial tensile tests were performed to investigate the mechanical properties of the GO/PAA/BPEI complexes from another perspective, helping to further understand their microstructure. As mentioned previously, not all the compositions were able to be tensile tested. Only when [PAA] = 44.1-57.9 wt % ($[PAA]_{sol}$ = 120-280 mM) in the materials can the tensile tests be performed due to the brittle nature of the complexes containing high GO content. Fig 5. shows three representative stress-strain curves for the complexes (the data for all other samples are shown in Fig S7a, ESI). As [PAA] in the complex increases from 44.1 to 52.9 wt% ($[PAA]_{sol}$ increases from 120 to 200 mM), the stress-strain curves exhibit a longer plateau showing that these materials undergo more plastic deformation. Then, when dried based PAA content further increase to 57.9 wt% ($[PAA]_{sol}$ increases from 200 to 280 mM), another transition is seen and the plastic deformation region became smaller.

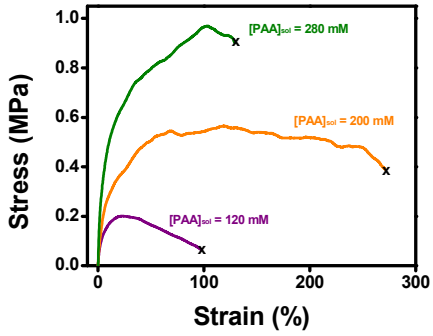

Fig 5. Stress-strain curves of GO/PAA/BPEI complex made from polyanion solution with $[PAA]_{sol}$ = 120 mM, 200 mM and 280 mM

Fig 6 illustrates the tensile properties obtained from the stress-strain curves as a function of [PAA]: tensile strength (σ_{max}), elastic modulus (E), strain at failure (ε_{max}) and toughness (U_T). Generally, as [PAA] increases, σ_{max} and E both increase as a result of the increasing crosslink density and decreasing swelling ratio; while U_T and ε_{max} first increase with increasing [PAA] until a maximum is reached at [PAA] = 52.9 wt%, then decrease when the [PAA] further increases.

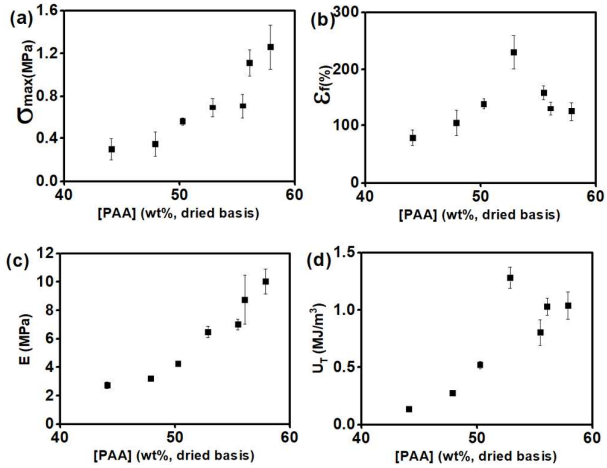

Fig 6. Tensile properties (a) tensile strength (σ_{max}); (b) failure strain (ε_{max}); (c) Young's modulus (E) (d) failure energy (U_T); of the GO/PAA/BPEI complex with [PAA] ranging from 40 wt% to 60 wt%

The variation in mechanical properties can be interpreted from consideration of the thermodynamics and kinetics of PEC formation. Earlier studies have suggested a two-step formation process for electrostatically driven complexes: the initial ionic clusters would form in the first step and a step of structural rearrangement follows, which involves exchange reaction between complex and the remaining macromolecules in the solution, allowing the growth and aggregation of the primary clusters.[33, 40, 41] The exchange process is highly dependent upon the nature of the charged molecules.[42] Having dimensions on the order of several microns,[27, 43] the 2D GO sheets are much larger in size than BPEI or PAA chains, which have a hydrodynamic radius on the order of several nanometers.[44, 45] Due to hindered size, shape, and flexibility, it is more difficult for GO sheets to participate in the exchange process in the same way that polyelectrolyte chains do. The presence of the GO sheets in the system may also locally hinder polymer diffusion. We postulate that, due to steric reasons, when the two oppositely charged polyelectrolytes are interacting a greater degree of crosslinking is achieved compared to the case of one polyelectrolyte and the large GO sheets. Hence, as [PAA] increases to 52.9 wt%, the strain at failure and the toughness increase, the plastic deformation region in stress-strain curve also becomes longer. However, as [PAA] further increases and the water content decreases, these mechanical properties are reduced. When [PAA] increases beyond 52.9 wt%: the strain at failure (ε_{max}) and the

toughness (U_T) decrease and the plastic deformation region becomes shorter.

Similarly, these changes in properties can be considered as a function of [GO] as shown in Fig S8 (ESI). Increasing [GO] decrease the maximum elongation and toughness (Fig S8b and Fig S8d) as expected from the inclusion of the stiff 2D material that may inhibit large scale, reversible rearrangements of the associative crosslinks. However, the tensile strength and elastic modulus are not monotonic with [GO]. At low loading ([GO] < 12.5 wt%), GO sheets are well dispersed amongst the polymer chains and offer effective improvement of mechanical properties. At higher loading of GO ([GO] > 12.5 wt%), the tensile strength and elastic modulus decrease with increasing [GO], which is counter to expectations from nanocomposite reinforcement. However, the GO may agglomerate at high concentrations and this would weaken the mechanical properties.[46]

3.4 Comparison to binary systems of GO/BPEI and BPEI/PAA

Comparison studies to analogous binary systems can be helpful for understanding the influence that each component has on the mechanical properties of the ternary complexes. As discussed earlier, for the GO/PAA/BPEI complex with low [PAA], G' is always greater than G'' (Fig 4c). However, the incorporation of the PAA chains changes the network and gives it a more viscous response upon oscillatory shear. Hence, unlike the GO/BPEI complex (i.e. $[PAA]_{sol} = 0$), which has G' and G'' values that are nearly independent of frequency (Fig S9a.), both G' and G'' of the GO/PAA/BPEI complex increase with frequency. For a stoichiometric BPEI/PAA complex (molar ratio of BPEI : PAA = 1.07, according to the ^{1}H NMR spectra), G' is slightly smaller than G'', consistent with viscoelastic liquid-like behaviour. After the being stored in DI for 60 days, the shape of a molded BPEI/PAA deforms significantly and flows under the influence of gravity at long times, which is consistent with liquid-like behavior. The addition of GO changes the visco-elastic properties of these materials substantially. Even for samples that have the highest polymer content ([GO]= 11.6 wt%), their molded shape is retained after 60 days in water (Fig S10), which clearly demonstrates the role of GO in inhibiting flow of the complex.

Table 2. Mechanical properties and swelling ratio of ternary and binary complexes

	GO/PAA/BPEI	BPEI/PAA	GO/BPEI
G' †	7.9-15.3 MPa	1.1 MPa	718.5 Pa
G'' †	2.2-13.7 Mpa	1.5 MPa	105.9 Pa
Tanδ†	0.28-0.93	1.36	0.15
σ_{max}	0.20-0.96 MPa	0.07 MPa	-
E	3.0-8.8 MPa	1.6 MPa	-
ε_{max}	97.5-271.2 %	715.8 %	-
U_T	0.14-1.04 MJ/m^3	0.15 MJ/m^3	-
q	1.4-3.7	1.6	71.8

† Rheological properties at 1 rad/s

Table 2 compares the mechanical properties and the swelling ratio of GO/PAA/BPEI complex with the binary systems. Though the small loss factor indicates the strong solid-like behaviour of the GO/BPEI complex, the shear modulus is also low and the material is too brittle to perform a tensile test. The GO/BPEI network interacts strongly with water leading to large water content, likely from uncompensated charges on BPEI. The strong interactions between PAA and BPEI and similarity in the local density of associating groups mean that the GO/PAA/BPEI network is much less swollen, leading to significantly different mechanical properties. The incorporation of GO in the polyelectrolyte complex does improve certain mechanical properties in comparison to the pure polyelectrolyte complex. Without GO, though the material has a much larger maximum elongation, the toughness of BPEI/PAA complex is only slightly larger than the toughness of the least tough GO/PAA/BPEI complex, and the shear modulus, elastic modulus, tensile strength are all much smaller for the binary BPEI/PAA than the ternary system with GO, indicating the mechanical strengthening effect offered by GO.

Conclusions

Bulk ternary GO/PAA/BPEI complexes were fabricated from a one-step solution precipitation process. Physical crosslinks formed from electrostatic interaction between GO and BPEI, as well as PAA and BPEI, in addition to physical entanglements of the polymers and 2D nanosheets, lead to viscoelastic solid-like or critical gel-like behaviour in the complexes. The incorporation of PAA can largely improve the processability of the GO/BPEI based complexes, most importantly reducing the brittleness of the complex. The ternary complexes can be molded and retain their desired shape when immersed in water for extended periods. The roles of GO and PAA in influencing the mechanical properties of GO/PAA/BPEI complexes were investigated: GO sheets can restrain the viscous flow of the complex and improve the mechanical strength at low loading (<12.6 wt%), but will decrease the mechanical properties when [GO] further increase. PAA chains more efficiently complexes with free hydrophilic functional groups on BPEI than GO to generate a less swollen and stronger network, but the incorporation of PAA increases the viscous losses of the complex. The understanding of ternary nanocomposite complexes provides guidance on effective routes to toughen and strengthen polyelectrolyte complex hydrogels or the bulk polyelectrolyte complexes.

Acknowledgements

This work was financially supported by NSF DMR 1425187 and ACS PRF 53739-ND7. We thank Prof. Mathew L. Becker of the University of Akron for the use of the die for samples preparation, Guodong Deng for his assistance with NMR experiments, Dr. Zhorro Nikolov for his help with Raman

spectroscopy and Yanfeng Xia for his assistance with FTIR measurements.

References

1. H. Dautzenberg, *Macromolecules*, 1997, **30**, 7810-7815.
2. Q. Wang and J. B. Schlenoff, *Macromolecules*, 2014, **47**, 3108-3116.
3. V. Y. Borue and I. Y. Erukhimovich, *Macromolecules*, 1990, **23**, 3625-3632.
4. Y. Hayashi, M. Ullner and P. Linse, *J. Phys. Chem. B*, 2003, **107**, 8198-8207.
5. K. S. Mayya, D. I. Gittins and F. Caruso, *Chem. Mater.*, 2001, **13**, 3833-3836.
6. A. C. Wan, B. C. Tai, K. J. Leck and J. Y. Ying, *Adv. Mater.*, 2006, **18**, 641-644.
7. C. Wang, Y. Duan, N. S. Zacharia and B. D. Vogt, *Soft Matter*, 2017, **13**, 1161-1170.
8. A. S. Michaels, *Ind. Eng. Chem.*, 1965, **57**, 32-&.
9. B. M. Wohl and J. F. J. Engbersen, *J. Controlled Release*, 2012, **158**, 2-14.
10. K. Ariga, Y. M. Lvov, K. Kawakami, Q. M. Ji and J. P. Hill, *Adv. Drug Delivery Rev.*, 2011, **63**, 762-771.
11. A. K. Sarker and J. D. Hong, *Langmuir*, 2012, **28**, 12637-12646.
12. F. Wu, J. Li, Y. F. Su, J. Wang, W. Yang, N. Li, L. Chen, S. Chen, R. J. Chen and L. Y. Bao, *Nano Lett.*, 2016, **16**, 5488-5494.
13. Y. H. Yang, L. Bolling, M. A. Priolo and J. C. Grunlan, *Adv. Mater.*, 2013, **25**, 503-508.
14. E. Ahn, T. Lee, M. Gu, M. Park, S. H. Min and B. S. Kim, *Chem. Mater.*, 2017, **29**, 69-79.
15. G. Decher and J. B. Schlenoff, *Multilayer Thin Films: Sequential Assembly of Nanocomposite Materials*, John Wiley & Sons, second edn., 2012.
16. K. C. Krogman, R. E. Cohen, P. T. Hammond, M. F. Rubner and B. N. Wang, *Bioinspiration Biomimetics*, 2013, **8**.
17. H. Bai, C. Li, X. L. Wang and G. Q. Shi, *J. Phys. Chem. C*, 2011, **115**, 5545-5551.
18. R. F. Shamoun, A. Reisch and J. B. Schlenoff, *Adv. Funct. Mater.*, 2012, **22**, 1923-1931.
19. H. Guo, T. Jiao, Q. Zhang, W. Guo, Q. Peng and X. Yan, *Nanoscale Res. Lett.*, 2015, **10**, 1-10.
20. Z. Y. Sui, Y. Cui, J. H. Zhu and B. H. Han, *ACS Appl. Mater. Interfaces*, 2013, **5**, 9172-9179.
21. H. Kim, R. Namgung, K. Singha, I. K. Oh and W. J. Kim, *Bioconjugate Chem.*, 2011, **22**, 2558-2567.
22. Z. Y. Xiong, C. L. Liao and X. G. Wang, *J. Mater. Chem. A*, 2014, **2**, 19141-19144.
23. J. P. Gong, *Soft Matter*, 2010, **6**, 2583-2590.
24. J. C. Fu, Q. F. Wang and J. B. Schlenoff, *Acs Applied Materials & Interfaces*, 2015, **7**, 895-901.
25. H. Zhang, C. Wang, G. Zhu and N. S. Zacharia, *ACS Appl. Mater. Interfaces*, 2016, **8**, 26258-26265.
26. A. Reisch, E. Roger, T. Phoeung, C. Antheaume, C. Orthlieb, F. Boulmedais, P. Lavalle, J. B. Schlenoff, B. Frisch and P. Schaaf, *Adv. Mater.*, 2014, **26**, 2547-2551.
27. D. C. Marcano, D. V. Kosynkin, J. M. Berlin, A. Sinitskii, Z. Z. Sun, A. Slesarev, L. B. Alemany, W. Lu and J. M. Tour, *ACS Nano*, 2010, **4**, 4806-4814.
28. K. N. Kudin, B. Ozbas, H. C. Schniepp, R. K. Prud'Homme, I. A. Aksay and R. Car, *Nano Lett.*, 2008, **8**, 36-41.
29. M. Naebe, J. Wang, A. Amini, H. Khayyam, N. Hameed, L. H. Li, Y. Chen and B. Fox, *Sci. Rep.*, 2014, **4**, 4375.
30. Y. Gu, Y. Ma, B. D. Vogt and N. S. Zacharia, *Soft Matter*, 2016, **12**, 1859-1867.
31. P. Schaaf and J. B. Schlenoff, *Adv.Mater.*, 2015, **27**, 2420-2432.
32. F. M. Lounis, J. Chamieh, P. Gonzalez, H. Cottet and L. Leclercq, *Macromolecules*, 2016, **49**, 3881-3888.
33. D. Priftis, X. X. Xia, K. O. Margossian, S. L. Perry, L. Leon, J. Qin, J. J. de Pablo and M. Tirrell, *Macromolecules*, 2014, **47**, 3076-3085.
34. J. Cho, J. F. Quinn and F. Caruso, *J. Am. Chem. Soc.*, 2004, **126**, 2270-2271.
35. Z. X. Tai, J. Yang, Y. Y. Qi, X. B. Yan and Q. J. Xue, *RSC Adv.*, 2013, **3**, 12751-12757.
36. A. Reisch, P. Tirado, E. Roger, F. Boulmedais, D. Collin, J. C. Voegel, B. Frisch, P. Schaaf and J. B. Schlenoff, *Adv. Funct. Mater.*, 2013, **23**, 673-682.
37. R. Zhang, Y. Zhang, H. S. Antila, J. L. Lutkenhaus and M. Sammalkorpi, *J. Phys. Chem. B*, 2017, **121**, 322-333.
38. H. H. Hariri, A. M. Lehaf and J. B. Schlenoff, *Macromolecules*, 2012, **45**, 9364-9372.
39. H. H. Winter and F. Chambon, *J Rheol.*, 1986, **30**, 367-382.
40. A. Zintchenko, G. Rother and H. Dautzenberg, *Langmuir*, 2003, **19**, 2507-2513.
41. Y. P. Zhang, E. Yildirim, H. S. Antila, L. D. Valenzuela, M. Sammalkorpi and J. L. Lutkenhaus, *Soft Matter*, 2015, **11**, 7392-7401.
42. H. W. Jomaa and J. B. Schlenoff, *Langmuir*, 2005, **21**, 8081-8084.
43. D. R. Dreyer, S. Park, C. W. Bielawski and R. S. Ruoff, *Chem. Soc. Rev.*, 2010, **39**, 228-240.
44. I. H. Park and E. J. Choi, *Polymer*, 1996, **37**, 313-319.
45. D. Reith, B. Muller, F. Muller-Plathe and S. Wiegand, *J. Chem. Phys.*, 2002, **116**, 9100-9106.
46. L. Zhang, Z. P. Wang, C. Xu, Y. Li, J. P. Gao, W. Wang and Y. Liu, *J. Mater. Chem.*, 2011, **21**, 10399-10406.

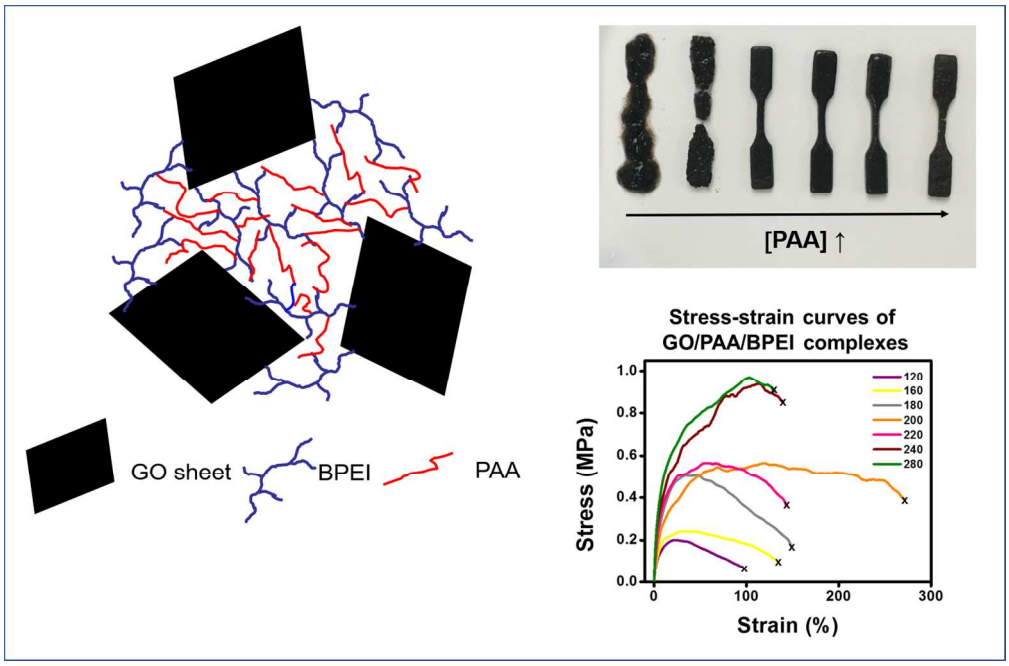
GO sheet
BPEI
PAA
[PAA] ↑
Stress-strain curves of
GO/PAA/BPEI complexes
Stress (MPa)
Strain (%)
120
160
180
200
220
240
280
0.0
0.2
0.4
0.6
0.8
1.0
0
100
200
300